Self-Assembling Behavior of Living Polymers

Jörg Stellbrink,* Lutz Willner, Olaf Jucknischke, and Dieter Richter

Institut für Festkörperforschung, Forschungszentrum, Jülich GmbH, Jülich, Germany D-52425

Peter Lindner

Institute Laue-Langevin, 156 Avenue des Martyrs, F-38042 Grenoble, Cedex 9, France

Lewis J. Fetters and John S. Huang

Corporate Research Laboratories, Exxon Research and Engineering Company, 1545 Route 22 East, P.O. Box 998, Annandale, New Jersey 08801-0998

Received December 30, 1997; Revised Manuscript Received April 21, 1998

ABSTRACT: In order to elucidate the structure of intermediate species present during the early stages of "living" anionic polymerization, the aggregation behavior of styryllithium head groups [$RCH_2CH^-(C_6H_5)Li^+$] in benzene was investigated by small angle neutron scattering (SANS). The monofunctional lipophobic anionic head group was found to self-assemble in a first step to dimers and tetramers. The concentration dependent equilibrium between these species was quantitatively analyzed by using the form factors of a Gaussian linear coil and star, respectively. These results seem to contradict a mechanistic viewpoint of anionic polymerization that dates to 1960. Therein the dimer was assumed to be the maximum allowable aggregation state for this head group. In addition, the SANS technique has shown that the intermediate scale structures can also form large scale self-assembled aggregates ($R_g \cong 10^3$ Å) whose scattering behavior can be analyzed in terms of a form factor for a mass fractal structure recently proposed by Beaucage.

Introduction

In a previous publication Fetters et al.[1] studied the self-assembling behavior of the styryl- and butadienyllithium head groups where the base chain was polystyrene. The techniques used included static light scattering (SLS), dynamic light scattering (DLS), and small angle neutron scattering (SANS). That work was the first to use the modern scattering techniques of DLS and SANS to investigate the structural properties of the self-assembled lipophobic anionic head groups present during polymerization. The authors found evidence for the presence of intermediate-sized aggregates in coexistence with larger scale structures with minimum aggregate sizes of 10^3 Å. On the basis of the SLS and DLS results, it was conjectured that the large scale structures were cylindrical (wormlike) micelles where the skeletal backbone is an alternating structure composed of carbon and lithium. The SANS evaluation was limited in the range of the scattering vector **Q** and thus able to capture only some indication of the presence of intermediate and the larger scale aggregates. That gap in **Q** range has been rectified in this work where the range now covers two decades. Furthermore, by a systematic study of the concentration dependent scattering profiles, the scattering patterns could be evaluated on an absolute scale. This permits a more extensive portion of the signature of these large aggregates to be accessed, thus allowing a more detailed assay of their structures.

The existing[1] experimental results seem to contradict a well-established mechanism[2] that dictates that the dimer (for the styryl head group) and tetramer (for dienyl head groups) aggregates are the maximum allowable aggregation states for each active center. This commonly accepted mechanism[2−4] is based upon a series of interdependent premises, to wit; the aggregated head groups are unreactive in the propagation reaction, while antithetically, the sole reactive species were presumed to be the singlet head groups. Thus, as a necessary consequence, the active singlet chains must arise from a labile association−dissociation event, which momentarily allows the carbon−lithium head group to indulge in propagation.

SANS directly investigates the microscopic details of the scattering particles with a resolution of several angstroms. It is thus the ideal tool for illuminating the structural properties of the intermediate-sized aggregates. This paper is concerned with the experimental details and the basic principles of our analysis scheme; i.e., distinct form factors are introduced, which are used to describe the scattering data for two decades in **Q**. The main point addressed will be the scattering properties of the aggregates and the principles of the data analysis. Thus the focus will be on the SANS-based data of the styryllithium active center, which shows the simplest behavior of the carbon−lithium-based head groups investigated. The SANS- and DLS-based results concerning the behavior of the dienyllithium and alkoxylithium head groups will be presented in subsequent papers.

Experimental Section

a. Sample Synthesis and Evaluation. The basic high-vacuum synthetic protocols and routines used for the preparation of samples for the scattering measurements were those described previously.[5] The vacuum was achieved and maintained by a Leybold mechanical roughing pump coupled to a turbo unit. Freshly prepared initiator (*sec*-butyllithium) was used. The initiator was prepared in pentane at 273 K from lithium dispersion and *sec*-butyl chloride. The temperature used minimized the Wurtz coupling event. Prior to the reaction, the lithium was washed free of the paraffin used to encapsulate the dispersion. The resultant initiator solutions

* To whom correspondence should be addressed.

S0024-9297(97)01890-1 CCC: $15.00
Published on Web 06/13/1998

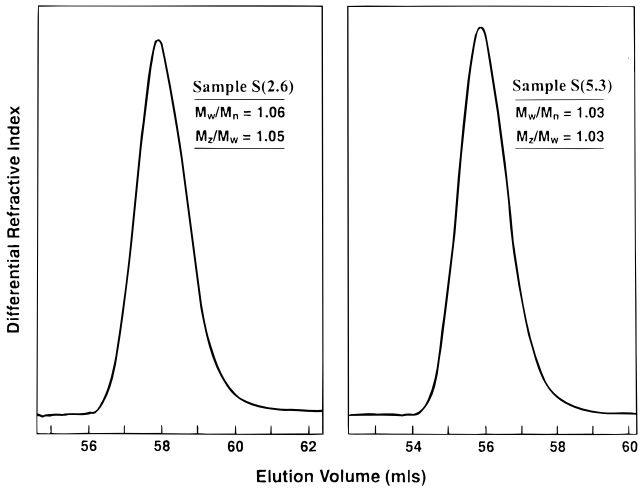

Figure 1. SEC traces of the terminated polystyrene sample S(2.6), $M_w^{SEC} = 2650$, and S(5.3), $M_w^{SEC} = 5288$.

were clear and colorless. The Gilman−Cartledge double titration techique[6] was used to assay the concentration of carbon-bound lithium. No evidence for the presence of non-carbon-bound lithium was revealed by this dual titration procedure. Exchange to the deuterated solvent was done prior to use. The initiator solutions were kept at ca. 258 K. That temperature prevents the spontaneous decomposition event, which leads to the evolution of lithium hydride and the 1- and 2-butene isomers.[7]

Since neutron scattering is sensitive to the coherent scattering length differences existing between hydrogen and deuterium hydrocarbon chain, micelles can be studied in solution when the solvent is labeled with one of the isotopes and the solute is labeled with the other. This variation in contrast then leads to coherent scattering intensity, $I(\mathbf{Q})$, by the solute. Perdeuteriobenzene was used as the solvent, while the base chain was prepared from styrene-h_8. The purification procedure involved solvent exposure to styryllithium and monomer exposure to dibutylmagnesium prior to collection by distillation. The benzene solutions were measured at room temperature. The combination of deuterated solvent and hydrogenous polymer was selected since it is known[8] that the **Q** independent incoherent scattering from deuterated solvents is about a decade less intense than that of their hydrogenous counterparts. The monomer was distilled directly into the reactor, a procedure designed to eliminate the presence of thermally prepared high molecular weight material in the final solutions. A high molecular weight component can form in the neat monomer over storage time even at ca. 258 K. Quartz cells of 2 and 5 mm path length were used for the SANS calibration and measurements. Those cells were attached to the reactor and, when filled, removed by heat sealing the interconnecting Pyrex tube.

The calculated radii of gyration, R_g, are based on the literature-based power laws given elsewhere.[9] Polymer concentrations were below the overlap concentration, c^*, of the dimer. That parameter was calculated via the following: $c^* = 3/(4\pi R_g^3)\, M_w/N_A$, where N_A is the Avogadro number. Molecular weights of the terminated polymers were measured via SANS and size exclusion chromatography (SEC); see Figure 1. The latter measurements yielded the apparent M_z/M_w and M_w/M_n ratios, which were no greater than 1.06. These values were not corrected for column-broadening effects. Thus the authentic values were <1.06. The base chains had molecular weights (SEC) of 2.65×10^3 and 5.3×10^3. Sample identification follows the previous format[1] involving the head-group identity and the molecular weight of the base polystyrene chain; e.g., SLi(2.6) denotes the styryllithium head group attached to the 2.65×10^3 base polystyrene chain.

b. SANS. In general, the macroscopic coherent scattering cross section[10] of a polymer solution observed by SANS can be expressed as

$$\left(\frac{d\Sigma}{d\Omega}\right)_{coh} = \frac{1}{N_A}\Delta\rho^2 I(\mathbf{Q})_p \tag{1}$$

The scattering vector **Q** is given by $4\pi\lambda^{-1}\sin(\theta/2)$ with θ the scattering angle and λ the neutron wavelength. $\Delta\rho^2$ is defined as the contrast factor between the polymer and the solvent:

$$\Delta\rho^2 = \left(\frac{\Sigma b_p}{\vartheta_p} - \frac{\Sigma b_s}{\vartheta_s}\right)^2 \tag{2}$$

Σb_s and Σb_p are the coherent scattering lengths, and ϑ_s and ϑ_p, the volumes of the solvent molecule and the repeat unit, respectively. $I(\mathbf{Q})_p$, the static scattering function, is related to the microscopic structure of the polymer by

$$I(\mathbf{Q})_p = \frac{1}{N}\sum_{i,j}^{N}\langle \exp[i\mathbf{Q}(r_i - r_j)]\rangle \tag{3}$$

where N is the total number of scatterers (i.e., for a polymer, the repeat units) and r_i and r_j are the positions of scatterers i and j, respectively. The static scattering function can also be expressed as a product of the intraparticle form factor, $P(\mathbf{Q})$, which describes the molecular architecture of the polymer, and the interparticle structure factor, $S(\mathbf{Q})$, which arises from the interactions between different polymer chains:

$$I(\mathbf{Q})_p = \Phi V_w\, P(\mathbf{Q})\, S(\mathbf{Q}) \tag{4}$$

with Φ the volume fraction of the polymer and V_w its weight average molecular volume. SANS experiments were performed at the Institut Laue-Langevin, Grenoble, France, using the D11 diffractometer. Detector settings of 2, 10, and 35.7 m and a neutron wavelength of $\lambda = 7$ Å resulted in an experimental **Q** range of 1.32×10^{-3} to 0.16 Å^{-1}. In general, all radial-averaged D11 data were normalized to a water standard according to the following formula, which yields the macroscopic scattering cross section of the solutions:

$$\left(\frac{d\Sigma}{d\Omega}\right)_{tot} = \left[\frac{[I_{sample} - I_{Cd}] - A_2[I_{ec} - I_{Cd}]}{[I_{H_2O} - I_{Cd}] - A_1[I_{ec} - I_{Cd}]}\right]\frac{A_3}{A_4} \tag{5}$$

The constants A_1−A_4 were determined from the intensities of the transmission measurements: $A_1 = I_{H_2O}/I_{ec}$, $A_2 = I_{sample}/I_{ec}$, $A_3 = (I_{H_2O}/I_{eb})l_{H_2O}(d\Sigma/d\Omega)_{H_2O}$, $A_4 = (I_{sample}/I_{eb})l_{sample}$, with I = intensity (counts/s), Cd = Cadmium run ("dark" counts), ec = empty cell, eb = empty beam, l = path length (2 and 5 mm), and $(d\Sigma/d\Omega)_{H_2O} = 0.886$ cm^{-1} at 7 Å. In addition, the 2 m data have been corrected for detector dead time effects. Finally, contributions due to incoherent background and solvent scattering have been subtracted from all data sets. The coherent scattering lengths have been calculated to be $\Sigma b_p = 2.33 \times 10^{-12}$ cm for styrene and $\Sigma b_s = 7.99 \times 10^{-12}$ cm for benzene-d_6. Thus, using, $d_{ps} = 1.04$ g cm^{-3}, $d_{bz} = 0.95$ g cm^{-3}, $M_{styrene} = 104$ g mol^{-1}, and $M_{bz} = 84$ g mol^{-1} yields a contrast factor $\Delta\rho^2 = 1.63 \times 10^{21}$ cm^{-4} for protonated polystyrene in benzene-d_6.

All experiments were performed at room temperature. Four different concentrations of the living polymers have been prepared, i.e., 0.1, 0.075, 0.05, and 0.025 g cm^{-3}. The solutions were transferred directly from the reactor into the sample cells after successive dilution under high-vacuum conditions. In order to have an exact calibration standard for the living polymer solutions, the solutions of the terminated polymer have been prepared separately by weight, ranging from 5.6×10^{-3} to 0.10 g cm^{-3}. Because of the experimental conditions needed for the polymerization, each dilution in the reactor results in an estimated error of ±4% on each concentration. Thus, the concentrations given above are the nominal values. These nominal concentrations have been calibrated relative to the terminated solutions by making use of the independence of the normalized intensities $I(\mathbf{Q})/\Phi$ on concentration in the high **Q** region, where the scattering arises solely from the connected repeat units of the polymer. The results of this

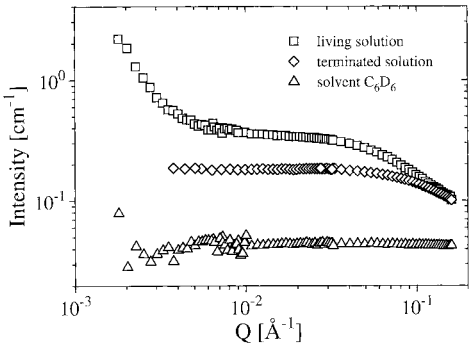

Figure 2. Scattering intensity (raw data) vs scattering vector **Q** for the terminated polystyrene sample S(2.6) and the corresponding living polymer SLi(2.6) at volume fractions $\Phi_{cal} = 2.4 \times 10^{-2}$ and 2.64×10^{-2}, respectively. Also shown are the data of the pure solvent C_6D_6.

Table 1. Volume Fraction "Calibration" of the Styryl Head Group Sample SLi(2.6)

sample	c (g/cm^3)	Φ_{nom} (%)	Φ_{cal} (%)	$\Delta\Phi$ (%)
SLi(2.6) A	0.01	9.62	9.40	2.3
SLi(2.6) A75	7.5×10^{-2}	7.21	7.05	2.3
SLi(2.6) A5	5.0×10^{-2}	4.81	5.20	8.1
SLi(2.6) A25	2.5×10^{-2}	2.40	2.64	10.0

calibration procedure are given in Table 1. Although the relative error increases with decreasing concentration, the agreement between the nominal and calibrated concentrations is reasonable. The transmissions of the different samples varied between 54 and 65 % for the living and between 55 and 70 % for the terminated solutions.

Results

a. Qualitative Scattering Patterns. Figure 2 displays SANS results from a living polymer solution, sample SLi(2.6) at a volume fraction of $\Phi_{cal} = 2.64 \times 10^{-2}$. For comparison, the data from the corresponding terminated solution ($\Phi = 2.4 \times 10^{-2}$) and the pure solvent are shown. These are raw data and have been corrected only for background and are normalized to water according to eq 5. While the solvent data remain flat over the entire **Q** range, the terminated solution follows a typical form factor for a linear chain of low molecular weight. The $I(\mathbf{Q})$ for the living polymer solution on the other hand coincide only at high **Q** with the terminated solution. At intermediate **Q** values the scattering profile develops a plateau well above that of the terminated chains, indicating the existence of aggregated species (first level aggregates). Striking indeed is the additional increase of scattering intensity at low **Q** for the living polymer. This is evidence for the presence of large scale structures, whereas the data obtained from the terminated polymer remain at the plateau value characteristic of the Zimm regime. This increase in intensity at low **Q** is an inherent property of living polymer solutions and indicates the existence of two well-separated characteristic length scales that must be taken into account when analyzing the data. The presence of the two disparate length scales was previously found[1] via the combination of SANS and DLS.

How different these length scales have to be is shown in a simple exercise involving the **Q** dependent simulated intensities from Debye chains[11] of different sizes. Figure 3 displays these scattering profiles from three monodisperse Debye chains present in equal amounts (weight percent). The mid-**Q** range (about 5×10^{-3} to 2×10^{-2} Å^{-1}) is characterized by a near-plateau in $I(\mathbf{Q})$. This is a consequence of the absence of structures having radii of gyration in the gap between 60 and 1500 Å. A similar behavior is seen in Figure 2.

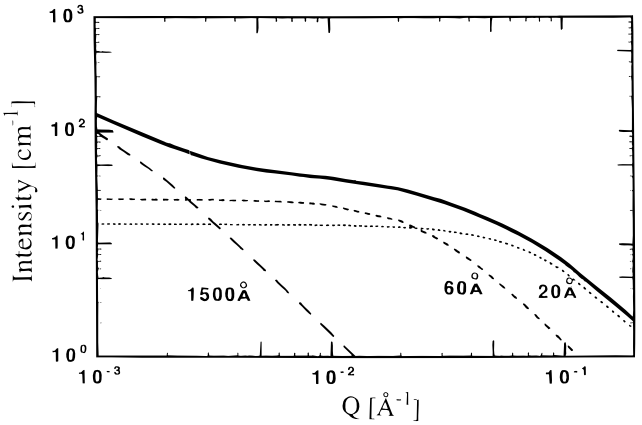

Figure 3. Simulated $I(\mathbf{Q})$ based upon three monodisperse Debye chains present in equal amounts (wt %). The numbers denote the radii of gyration.

b. Model Form Factors. In order to describe the scattering data from polymer solutions, i.e., the forward scattering $I_{\mathbf{Q}\to 0}$ and the shape of $I(\mathbf{Q})$ vs **Q**, several approaches have been made. From an extrapolation to zero concentration and the $\mathbf{Q} \to 0$ limit the Zimm plot yields the radius of gyration R_g, the weight average molecular volume V_w, and the second virial coefficient A_2.

$$\left(\frac{\Phi}{\lim_{\mathbf{Q}\to 0} I(\mathbf{Q})}\right) = \left(\frac{1}{V_w} + 2A_2\Phi + \frac{1}{V_w}\frac{R_g^2\mathbf{Q}^2}{3}\right) \qquad \mathbf{Q}R_g \le 1 \tag{6}$$

To account for the complete **Q** dependence of the scattering intensity, the explicit form factor of the aggregating polymers is needed. This can be calculated analytically by starting from eq 3 for some special aggregate structures. One of the simple types of aggregate is that of a polymer star. Benoît[12] calculated the form factor for an f-functional Gaussian star:

$$P(\mathbf{Q}) = \frac{2}{f\mathbf{Q}^4 R_{g,arm}^4}\left[\mathbf{Q}^2 R_{g,arm}^2 - (1 - e^{-\mathbf{Q}^2 R_{g,arm}^2}) + \frac{f-1}{2}(1 - e^{-\mathbf{Q}^2 R_{g,arm}^2})^2\right] \tag{7}$$

However, with increasing complexity of the aggregate structure, the mathematical effort to derive $P(\mathbf{Q})$ becomes formidable and/or the equations can no longer be expressed analytically. Another difficulty relates to the excluded volume interaction leading to chain swelling. For example, the loss of Gaussian statistics prevents an analytic solution of eq 3 even for a linear chain. Hence, semiquantitative expressions have been developed,[13] e.g., the form factor of a swollen star.

Another possible aggregate structure is that of a Gaussian comb,[14] where the living head groups would form a chain. If we consider an aggregate structure based on such an alternating chain of carbon and lithium atoms (the backbone) from which f arms (the polystyrene chains) of length n_b start, from each carbon atom one arm, the comb-form factor may be modified in such a way that it contains only one free parameter,

the aggregation number f, while all other parameters can be expressed by the following relations:

- n_b number of atoms in the side chain (n_b = is given by the molecular weight of the terminated chain)
- number of atoms in the backbone $N_0 = 2f$ (per chain one carbon and one lithium atom)
- total number of atoms $N = 2f + f(n_b - 1) = f(n_b + 1)$
- the ratio of backbone to the total number of atoms:

$$\lambda = N_0/N = 2/(1 + n_b)$$

- bond length b, ~2.15 Å[15,27]
- furthermore, we have introduced an arbitrary amplitude factor A for taking into account concentration and interaction effects. Thus we obtain the following equation:

$$P(\mathbf{Q}) = \frac{2A}{u^2}\left[u - t_1 + t_2(f + 2t_3/t_4) + {t_2}^2\left(\frac{(f-1)t_5 - t_6}{(t_5)^2}\right)\right] \quad (8)$$

where the dimensionless variable $u = \mathbf{Q}^2 f(n_b + 1)b^2/6$ and t_i is defined as follows:

$$t_1 = 1 - \exp[-2u/(1 + n_b)]$$

$$t_2 = 1 - \exp\left[-u\left(1 - \frac{2}{(1 + n_b)}/f\right)\right]$$

$$t_3 = 1 - \exp\left[-\frac{2uf}{(1 + n_b)(f + 1)}\right]$$

$$t_4 = 1 - \exp\left[-\frac{2u}{(1 + n_b)(f + 1)}\right]$$

$$t_5 = \exp\left[\frac{2u}{(1 + n_b)(f + 1)}\right] - 1$$

$$t_6 = 1 - \exp\left[-\frac{2u(f-1)}{(1 + n_b)(f + 1)}\right] \quad (9)$$

One additional possibly interesting structure is the Kratky−Porod wormlike chain model, the (asymptotic) form factor of which was recently given by Egelhaaf and Schurtenberger[16] and also by Brulet et al.[17] This form factor failed to give an accurate description of the living polymer scattering profiles; e.g., this model demands a fractal dimension (see below) of about 2 in the low **Q** range. Another approach has been recently taken by Beaucage,[18−20] who proposed a "universal form factor" for an arbitrary mass fractal, avoiding numerical integration, that can also be applied to polymeric systems:

$$P(\mathbf{Q}) = G\exp(-\mathbf{Q}^2{R_g}^2/3) + B\left(\frac{1}{\mathbf{Q}^*}\right)^P \quad (10)$$

with $\mathbf{Q}^* = \mathbf{Q}/[\mathrm{erf}(\mathbf{Q}kR_g/\sqrt{6})]^3$. Herein erf is the error function and G and B are amplitudes, which for mass fractals can be related to each other $B = GP/{R_g}^P\,\Gamma(P)$ (polymeric constraint). P is the (mass) fractal dimension of the internal substructure, k is an empirical constant found to be ≈ 1.06, and Γ is the Gamma function. The first term of eq 10 corresponds to a conventional Guinier approach describing the overall properties of the scatterers observed at low **Q**. Scattering contributions due to the internal substructure, which will be resolved at higher **Q**, are described in the second term. This term goes to zero when **Q** approaches zero, a great advantage of eq 10 compared to, e.g., the Dozier function.[13] At large **Q** the error function term describes the asymptotic power law $I \sim \mathbf{Q}^{-P}$. It has been shown that eq 10 describes results derived by numerical integration within very small errors.[18] Moreover, eq 10 can be extended to describe the scattering from structures with an arbitrary number n of substructural levels (the following expression is valid for $n = 2$):

$$I(\mathbf{Q}) = G\exp(-\mathbf{Q}^2{R_g}^2/3) + B\exp(-\mathbf{Q}^2{R_{sub}}^2/3)\left(\frac{1}{\mathbf{Q}^*}\right)^P + G_s\exp(-\mathbf{Q}^2{R_s}^2/3) + B_s\left(\frac{1}{\mathbf{Q}_s^*}\right)^{P_s} \quad (11)$$

with $\mathbf{Q}^* = \mathbf{Q}/[\mathrm{erf}(\mathbf{Q}kR_g/\sqrt{6})]^3$ and $\mathbf{Q}_s^* = \mathbf{Q}/[\mathrm{erf}(\mathbf{Q}kR_s/\sqrt{6})]^3$, respectively. G, B, G_s, and B_s are amplitudes, and again, use of the polymeric constraints can relate the different amplitudes to reduce the number of parameters. The initial term in eq 11 describes the large scale structure of size R_g composed of smaller scale building blocks of size R_s, captured in the third term. The second term describes the mass fractal regime of the large scale structure with two structural limits. The low-**Q** limit is at R_g and is described by the error function, which goes to zero when **Q** approaches zero. The high-**Q** limit is at R_{sub} and is described by the exponential prefactor, which cuts off the asymptotic power law of the error function term. The final term describes the internal fractal structure of the smaller scale building blocks. The assumption that $R_{sub} = R_s$ should always be true for typical mass fractals.

c. Quantitative Analysis. For a quantitative assay of the SANS data of aggregating living polymers an exact determination of the molecular parameters of the corresponding terminated polymers, which are the smallest building blocks of the aggregates, is a prerequisite. Thus, the terminated solutions are discussed in some detail before we focus on the structure of the aggregates. We applied, what we call, a "generalized Zimm plot", i.e., fitting the scattering data of several concentrations simultaneously, to

$$I(\mathbf{Q}) = \frac{\Phi(1 - \Phi)}{[1/(V_w P(\mathbf{Q})) + 2A_2\Phi]} \quad (12)$$

Since the concentration regime under study extends to relatively high volume fraction Φ, the "correct" concentration term of the RPA[21] approach has to be used, i.e., $\Phi(1 - \Phi)$ instead of the Φ approximation commonly used.

Due to the low molecular weight of the polymers under study the corresponding low R_g values give only weak slopes in a conventional Zimm diagram, which are difficult to analyze. In addition, due to the low molecular weight, excluded volume interactions are not effective. Thus the Debye function could be used to describe the form factor over the entire **Q** range; see Figure 4. We also tried to use the Beaucage form factor, eq 10, with $P = 2$, to describe the experimental data. The resulting parameters of the different analysis methods are summarized in Tables 2 and Table 3. As can be seen, all experimental data are well described by both form factors and the resulting fit parameters

Table 2. Molecular Characteristics of Terminated Polystyrene Sample S(2.6)

	conv Zimm	Beaucage	Debye	SEC
M_w	2332 ± 60	2440 ± 13	2442 ± 13	2650
M_w/M_n				1.06
R_g (Å)	7.45 ± 1.1	15.2 ± 0.1	15.2 ± 0.1	
A_2 (cm^3 mol/g^2)	(2.53 ± 0.12) × 10^{-3}	(2.47 ± 0.03) × 10^{-3}	(2.47 ± 0.03) × 10^{-3}	
P_s		2		

Table 3. Molecular Characteristics of Terminated Polystyrene Sample S(5.3)

	conv Zimm	Beaucage	Debye	SEC
M_w	4742 ± 60	4802 ± 75	4826 ± 65	5228
M_w/M_n				1.03
R_g (Å)	24.0 ± 0.5	22.4 ± 0.2	22.5 ± 0.3	
A_2 (cm^3 mol/g^2)	(1.91 ± 0.08) × 10^{-3}	(1.67 ± 0.04) × 10^{-3}	(1.68 ± 0.04) × 10^{-3}	
P_s		2		

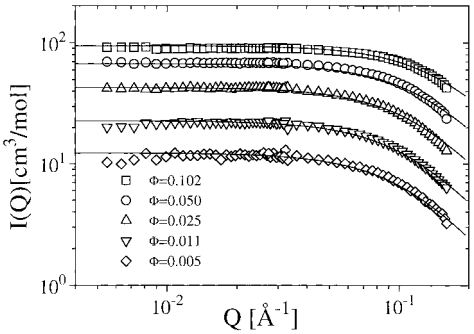

Figure 4. Scattering intensity vs scattering vector **Q** for the terminated polystyrene sample S(2.6). The volume fractions Φ are 1.02 × 10^{-1}, 4.99 × 10^{-2}, 2.48 × 10^{-2}, 1.11 × 10^{-2}, and 5.56 × 10^{-3} from above. The solid lines are the fit results of eq 12 with P(**Q**) given by the Debye function. Also shown are the results obtained by a conventional Zimm analysis (dotted lines).

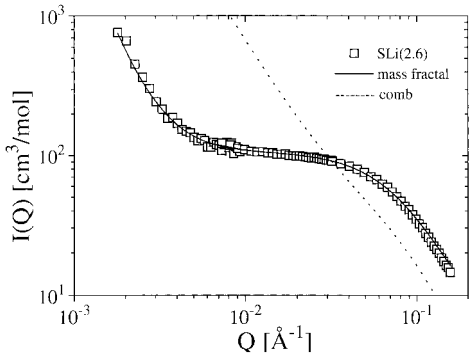

Figure 5. Fitting I(**Q**) of the living polymer SLi(2.6) solution with Φ_{cal} = 2.64 × 10^{-2} to the extended mass fractal form factor, eq 11, yielding a nearly perfect description of the data. The obtained parameters are listed in Table 4. Also shown is I(**Q**) calculated according to the modified comb from factor, eq 8, with parameters given by the terminated polystyrene chain S(2.6) (see text).

are nearly identical. The agreement between the SEC and SANS molecular weight results are well within experimental error.

For the lowest molecular weight the second virial coefficient A_2 obtained from our SANS data is surprisingly high compared to previous work.[22] But one should notice that those authors reported that A_2 obtained from SANS was always considerably higher than A_2 obtained from static light scattering, especially in the low-M_w region. Already for the next higher M_w we found a reasonable agreement between those and our data. The analysis of the SANS data took place in several steps. First the terminated solutions were evaluated, leading to second virial coefficients for PS(2.6) and PS(5.3) (model chain for the dimer). Then the living polymer data were parametrized by a fit to the Beaucage form factor. Finally, the concentration effects are also considered for the living system, using the virial coefficient from the terminated solutions.

In order to parameterize the scattering behavior of the living polymer solutions, we made a first attempt of fitting the experimental data of each concentration separately to the extended mass fractal form factor, eq 11. The amplitudes G and G_s, particle radii R_g and R_s and the fractal dimension P of the large scale aggregates are used as free parameters, whereas the internal fractal dimension of the subunits is fixed to P_s = 2 (Gaussian coil). The resulting fit for the lowest concentration Φ_{cal} = 2.64% is shown in Figure 5. As can be seen, the experimental data are well described by this model over the whole experimental **Q** range. The results obtained for the different concentrations are summarized in Table 4. Although this is merrily a

Table 4. Results of Fitting the Complete Q Range of Sample SLi(2.6) to the Mass Fractal Form Factor

	volume fraction Φ_{cal}			
	2.64%	5.2%	7.05%	9.4%
G (cm^3/mol)	5926	3421	507	688
R(Å)	1658	1329	904	902
P	2.92	3.1	3	2.8
G_s (cm^3/mol)	107	148	159	155
R_s (Å)	22.2	19.2	17.7	14.0
P_s	2	2	2	2

preliminary semiquantitative analysis, the following conclusions can already be drawn:

(i) The measured fractal dimension $P \approx 2.9$ for the large scale aggregates is surprisingly high for a polymer system, indicating a very dense, i.e., highly branched, structure.

(ii) Although no crossover to a Guinier regime at low **Q** is visible, we still can give a lower limit for the radius of gyration of the large aggregate. Their size must be *at least* ≈10^3 Å. This becomes clear by looking more closely at the properties of the power law tail described by the error function terms in eqs 10 and 11, respectively. For illustration, in Figure 6 I(**Q**) data are shown calculated according to eq 10 with different sets of parameters G, R_g, and P. In the high-**Q** range, where only power law behavior is observed, one cannot distinguish between the two parameter sets. The parameter R_g determines solely the crossover from the power law regime to the Guinier regime at low **Q**. Thus, we *cannot* determine the molecular weight of the aggregates because our experimental data do not reach the Zimm regime of the large scale aggregates. Nev-

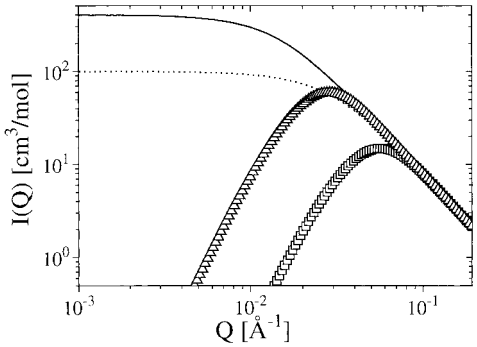

Figure 6. Scattering intensity vs scattering vector **Q** calculated according to the mass fractal form factor, eq 10, for two sets of parameters: (dotted line, squares) $G = 100$ cm^3 mol^{-1}, $R_g = 50$ Å, $P = 2$; (solid line, triangles) $G = 400$ cm^3 mol^{-1}, $R_g = 100$ Å, $P = 2$. The open symbols denote the scattering contributions due to the internal substructure, i.e., the second term in eq 10, which goes to zero when **Q** approaches zero.

ertheless, there exists a *minimum* combination of M_w and R_g to describe the observed power law tail.

(iii) The evaluated size of the first level aggregate, $R_s = 22.2$ Å, is nearly identical with the expected value of ≈21−24 Å for the dimer.[9] We note, however, that the second virial coefficient has not yet been taken into account at this level of analysis.

In addition, led by the idea that the head groups may associate in the form of long chains, an attempt was made to fit the experimental data to the symmetric comb form factor,[14] but eq 8 with the set of parameters given by the terminated chain does not describe the experimental data; see Figure 5. In principle, the comb form factor shows some similarities to the experimental data. If n_b and f are chosen very large, a plateau evolves in the mid-**Q** range, but varying f and n_b yields parameters not consistent with the chemical system, $n_b \approx 3000$ instead of ∼25. Moreover, the steep increase at low **Q**, where it is found that $I(\mathbf{Q}) \sim \mathbf{Q}^{-2.9}$, cannot be described by the comb form factor, which exhibits $I(\mathbf{Q}) \sim \mathbf{Q}^{-2}$. The same is true for the wormlike chain form factor, which also leads to $I(\mathbf{Q}) \sim \mathbf{Q}^{-2}$ at low **Q**.

For a more quantiative analysis of our experimental data we focus on the mid- and high-**Q** range, i.e., $\mathbf{Q} \geq 0.02$ Å^{-1}, where we reach a Zimm regime for the first level aggregates. As already mentioned in the Introduction, the commonly accepted polymerization mechanism for styrene assumes the dimer to be the maximum aggregation state. To calculate the forward scattering $I_{\mathbf{Q}\to 0}$ according to eq 12, three parameters are needed: the molecular weight M_w of the first level aggregates, their volume fraction Φ, and their second virial coefficient A_2. M_w and Φ are known from the characterization of the corresponding terminated polymer and the concentration calibration procedure, $M_w^{dimer} = 2M_w^{term}$ and $\Phi^{dimer} = \Phi^{cal}$, respectively. A_2 can be approximated by the value of the terminated sample *C*, for which M_w is approximately twice the value of the terminated low-M_w sample, i.e., $A_2 = 1.68 \times 10^{-3}$ cm^{-3} mol g^{-2}. Thus, in principle, all parameters are known with only R_g left as a fitting parameter (but it can be expected to be ≈$\sqrt{2}$·15.2 Å, the value of the terminated sample).

Figure 7 shows the comparison of our experimental data in the concentration range $0.0264 \leq \Phi \leq 0.094$ with the curves calculated according to eq 12 with $P(\mathbf{Q})$ given by the Debye function. Whereas the forward scattering at the highest concentration is reasonably described by

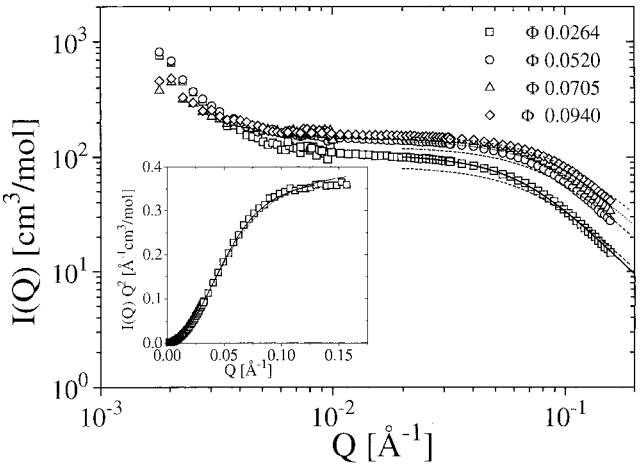

Figure 7. Scattering curves of the living polymer SLi(2.6) as a function of volume fraction Φ. The theoretical curves (dashed lines) are calculated according to eq 12 with $P(\mathbf{Q})$ given by the Debye function using M_w of the dimer and A_2 as the experimental value obtained from the terminated sample S(5.3). R_g is the only adjustable parameter (see text). Also shown is the curve assuming a mixture of dimers/tetramers (solid line) for the lowest concentration. The inset shows a Kratky representation for the lowest concentration, $\Phi = 2.64 \times 10^{-2}$, together with fitting results assuming only dimers (dotted line) or a mixture of dimers/tetramers (solid line).

this parameter set, the experimental intensity observed for the lower concentrations is much higher than calculated. For this effect there is only one possible explanation: a change in aggregate structure with concentration. The aggregation number increases with decreasing volume fraction; probably a mixture of dimers (Gaussian coils) and tetramers (Gaussian four-arm stars) is formed. To check this hypothesis, we analyzed the experimental data by

$$I(\mathbf{Q}) = \frac{\Phi_{tot}(1-\Phi_{tot})}{[1/(\Phi_{rel}^{star} P_{star}(\mathbf{Q}) + (1-\Phi_{rel}^{star})P_{debye}(\mathbf{Q}) + 2A_2\Phi)]} \quad (13)$$

with $\Phi_{rel}^{i} = \Phi_i/\Phi_{tot}$, Φ_i the volume fraction of component *i*, and Φ_{tot} the total polymer volume fraction. $P_{star}(\mathbf{Q})$ is given in eq 7. A_2 for the tetramer is taken to be approximately A_2^{dimer}.[23] The resulting fit for the lowest concentration, $\Phi_{cal} = 2.64 \times 10^{-2}$, is also shown in Figure 7. A relative star volume fraction $\Phi_{rel}^{star} = 0.45$ is needed to describe the forward scattering at this volume fraction. The concentration independent $R_g^{arm} \approx 17$ Å agrees with $R_g^{term} + 2.1$ Å, the expected value of a lithium−carbon bond.[15,27] Moreover, also the shape of $I(\mathbf{Q})$ is much better described by eq 13, as can be seen in the inset of Figure 7.

In principle, also other aggregation states like trimers or even unimers could be considered. The form factors arising from mixtures of these different aggregation states are very similar, and a definite decision on the presence of trimers or unimers or both cannot be given with certainty. However, the intermediate intensity level, which is above what would be expected for dimers only, requires the presence of aggregate numbers higher than 2. The presence of a sizable fraction of unimers, e.g., would imply an even higher relative amount of tetramers. We note, in addition, that unimers are not very favorable for enthalpic reasons.[28]

Table 5. Results of Fitting the Range $Q \geq 0.02$ Å^{-1} to a Sum of a Debye Function and a Gaussian Star with $f = 4$ (Dimer/Tetramer) for the Styryl Head Group of Sample SLi(2.6)

	volume fraction			
	2.64%	5.2%	7.05%	9.4%
Φ_{rel}^{star}	0.45 ± 0.01	0.40 ± 0.01	0.33 ± 0.02	0.11 ± 0.02
M_w^{star} (cm^3/mol)	9768[a]	9768[a]	9768[a]	9768[a]
R_g^{arm} (cm^3/mol)	17.5 ± 0.1	17.0 ± 0.1	17.3 ± 0.8	17.2 ± 0.1
M_w^{debye} (cm^3/mol)	4884[b]	4884[b]	4884[b]	4884[b]

[a] Fixed to M_w of a tetramer. [b] Fixed to M_w of a dimer.

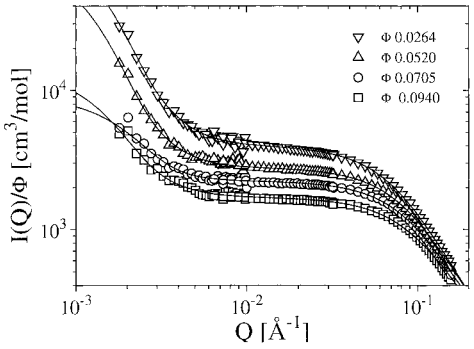

Figure 8. Fitting of the experimental data to a combination of the mass fractal form factor, eqs 10 and 13, yielding an excellent description of the experimental data.

Table 6. Results of Fitting the Complete Q range of sample SLi(2.6)

	volume fraction Φ			
	2.64%	5.2%	7.05%	9.4%
G (cm^3/mol)	3070 ± 430	4146 ± 634	486 ± 55	1152 ± 220
R_g (Å)	1268 ± 62	1410 ± 75	852 ± 55	1158 ± 92
P	2.98 ± 0.04	3.06 ± 0.06	3.11 ± 0.16	2.82 ± 0.07

The results for the other concentrations are listed in Table 5. Thus, at all concentrations we have mixtures of dimers and tetramers with Φ_{rel}^{star} decreasing with increasing concentration. Finally, after successfully describing the data in the mid- and high-**Q** range, we return to the low-**Q** regime, i.e., the large aggregates. In this step, eq 10 was added as an additional term to eq 13 to take into account the scattering contributions of the large scale aggregates. Whereas the parameters for the first level aggregates, i.e., dimers/tetramers, were fixed to the values obtained from the previous analysis step, G, R_g, and P of the large scale aggregates were used as free parameters; see Figure 8. As already mentioned above, no definite result can be obtained for the molecular weight of the large scale aggregate. G used in this way is not an explicit molecular volume but rather a factor containing all parameters affecting the forward scattering of the large scale aggregates, i.e., their concentration, their real V_w, and their second virial coefficient, respectively. But the obtained value of R_g is a minimum value needed to describe the upward curvature in I(**Q**) vs **Q**. Similarly, also the value for the prefactor G can be considered as a product of a minimal scattering volume V_w^{large} and the respective concentration Φ^{large}. The effect of a second virial coefficient would only increase the volume V_w^{large}. Data at lower **Q** would be needed in order to access the Zimm regime of these large scale structures. The results obtained are summarized in Table 6.

For the interpretation of these fits to the data there are two possible routes:

(i) One could assume that we deal in the sense of Beaucage with large aggregates built from smaller substructures. Thus, the scattering profiles seen at small and large **Q** originate from the same structure.

(ii) What is observed results from an equilibrium of different species containing singlet chains that make up the first level aggregates like dimers, tetramers, etc. in coexistence with the large scale structures.

Though we cannot give a definite value for the size of the large scale structures, we may estimate the fraction of chains contributing to these structures on the basis of their minimum size (see discussion above) and, thus, decide between the two possibilities discussed above. The estimate is performed using the absolute intensities obtained from the Beaucage fit for the two entities that directly relate to their scattering volumes V_w (eq 4). Let us first consider case i, the observation of homogeneous larger scale structures built from smaller entities. We take the data at $\Phi_{cal} = 2.64\%$ as a representative result. There the primary structures (first level aggregates), responsible for the mid-**Q** regime scattering, are mixtures of dimers and tetramers with an average volume $\overline{V_w} = 0.45V_w^{tetr} + 0.55V_w^{dimer} = 6800$ cm^3 mol^{-1}. On the other hand, the product of molecular volume and volume fraction of the large aggregates amounts to $V_w^{large}\,\Phi^{large} = G = 3070$ cm^3 mol^{-1}. With all monomers participating in the large scale structure $\Phi^{large} = \Phi_{cal}$ and $V_w^{large} = 116\,250$. Knowing V_w^{large}, we may calculate the number of small objects making up the large object and obtain $V_w^{large}/\overline{V_w} = 17$. It is noted that this result is obtained for the minimum size of $R_g = 1270$ Å required to explain the scattering pattern. Considering the vast difference in size between the small (≈25 Å) and the large structure ($R_g > 1270$ Å) the amount of scattering volume $V_w^{large} = 17\bar{V}_w$ is by orders of magnitudes too small. Thus, case i is ruled out.

The scattering pattern must, therefore, originate from an equilibrium between dimers and tetramers and, perhaps, a minor amount of unimers on the one hand and the large scale structures on the other hand. We now estimate the relative volume fraction of the monomers participating in the large scale structure. As derived from the fit, these large scale structures are mass fractals with $P \cong 3$. The underlying structure is rather densely packed and we estimate the number of entities building the large structure by $n = (R_g^{large}/R_g^{small})^3 \approx 10^5$ and $V_w^{large} \cong n\overline{V_w} \cong 10^9$ cm^3 mol^{-1}. In order to arrive at $G = \Phi_{large}V_w^{large} = 3070$, $\Phi_{large} = 3 \times 10^{-6}$ or $\Phi_{large}/\Phi = 1.2 \times 10^{-4}$ results. Thus, these large aggregates contain only a minor fraction of the monomers. We note that our estimate is based on the minimum aggregate sizes. Possible larger sizes will only reduce the fraction of large scale aggregates necessary to produce the observed scattering patterns.

Discussion

The lipophobic identity of the ionic head groups coupled with the lipophilic character of the hydrocarbon tails invites comparison with the micellization behavior exhibited by ionomers and surfactants. These systems[24,25] are well-known for their proclivities for self-organization into supramolecular structures, e.g., the canonic disk, spherical (star-shaped), and cylindrical-shaped micelles. The type of structures formed are the outcome of the interplay between the enthalpic contri-

bution resulting from the act of aggregation and head group packing preferences and the entropic considerations of the tails. The head group aggregation event necessitates a loss in translational freedom of the tail and thus a loss in entropy. The spontaneity of the association event dictates its exothermic identity. The structures formed can be viewed as polymer "bottle brushes",[26] and thus the entropy loss endured by the tails also includes that arising from chain stretching (the configurational entropy) in the aggregates. Compensation occurs via the aforementioned exothermic aggregation enthalpy, which for the dimer of allyllithium is judged[27] to be about 170 kJ.[28] That value is in keeping with the high ionic character of the head groups.[15]

As discussed above from the absolute intensities of the length scale dependent contributions to the scattering cross section, it is clear that we are faced with a delicate balance between a vast majority of dimers and tetramers, giving rise to the intermediate **Q** plateau in $d\Sigma/d\Omega$ and a very small fraction $\sim 10^{-4}\Phi$ of monomers aggregated in a large scale structure. Also photon-correlation spectroscopy on the butadienyllithium head group[1,29] confirms this general picture in showing clearly the coexistence of two primary diffusive relaxation modes. This signals the presence of two separate families of aggregated structures. Unfortunately, SLS and DLS techniques cannot be applied to the styryllithium head group in a quantitative fashion[30] due to the orange-red coloration of the solutions; $\lambda_{max} = 333$ nm in benzene[2] and 328 nm in cyclohexane.[31] This prevents the extension of the **Q** range to $<10^{-3}$ Å^{-1}, which is a prerequisite to reach the Zimm regime needed for a complete assay of the large scale structures. Thus, for this head group, SANS is the only applicable scattering technique.

From the concentration dependent height of the mid-**Q** plateau, the coexistence of two separate species, i.e., dimers *and* tetramers, was deduced. It should be again emphasized that only one adjustable parameter (the relative volume fraction of tetramers) was needed to describe the scattering data in the **Q** range of $0.02 \leq \mathbf{Q} \leq 0.2$ Å^{-1} for volume fractions $2.64 \times 10^{-2} \leq \Phi \leq 9.4 \times 10^{-1}$. With decreasing head group concentration, the relative volume fraction of tetramers increased from 0.11 ± 0.02 to 0.45 ± 0.01. The presence of the tetrameric structure is needed also to describe the functional shape of $I(\mathbf{Q})$ vs **Q**. In Figure 7 (insert) the experimental data and the fit according to eq 10 of the lowest concentration SLi(2.6K) sample is shown in the Kratky format, i.e., $I(\mathbf{Q})\mathbf{Q}^2$ vs **Q** (this representation emphasizes the data of the high-**Q** region). Also shown is the result of fitting the data to the Debye function. In order to achieve any agreement for this forced fit, the second virial coefficient had to be allowed to vary. Only in this fashion could the intensity of the mid-**Q** plateau be described. The resulting A_2 value of 4.4×10^{-4} mol cm^{-3} is about 1 order of magnitude too small.[9] This helps to highlight the inability of this attempt to adequately describe the scattering data. Moreover, the Debye function cannot describe the shape of the Kratky plot of the experimental data whereas the dimer/tetramer mixtures do. The characteristic feature of star polymer scattering data,[32−34] a peak in the Kratky representation, is not seen in Figure 7 due to the low functionality ($f = 4$) and the superposition of the Debye function (as will be seen in a subsequent publication,[29] the presence of such a peak plays an important role in the evaluation of the butadienyllithium head group data).

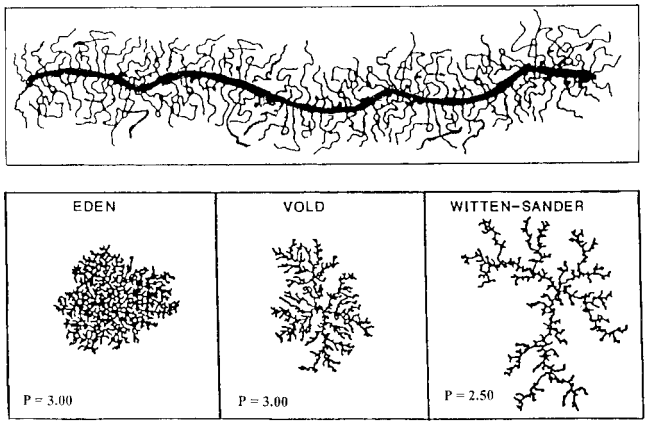

Figure 9. Possible fractal structures of the large scale aggregates and parent "bottle brush" chain. Each of the named fractal structures has its fractal dimension, *P*, given. These structures, which were generated by a simulation exercise (ref 39), each contain 10^3 primary units.

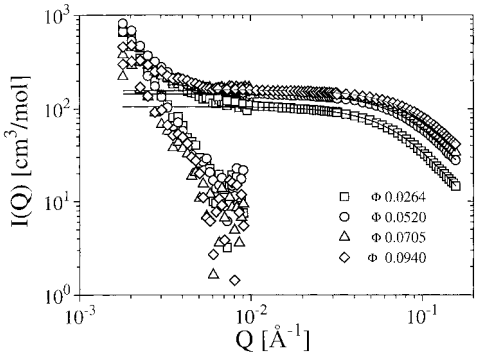

Figure 10. Scattering contribution of the large scale aggregates, i.e., the residual intensity after subtraction of the intensity calculated by eq 13, yielding a universal power law with slope ≈3.

The unambiguous presence of dimers and tetramers involving the styryllithium head group clearly contradicts the presently accepted mechanism, which demands that the dimer be the lone aggregation state in this system. The questionable nature of that mechanism was initially indicated as a consequence of a computer-based curve-fitting analysis[35] coupled with a graphical exercise;[36] both evaluations involved the head group concentrations and the propagation rate data for styrenic monomers. That mechanism further assumes the mantle of unreality by considering the second main finding of our study; namely, the existence of large scale aggregates. These are the structures[37,38] that give rise to the steep increase of the scattering intensity at low **Q**. The unexpected gradient steepness of about -3 is the reason for the failure of the form factors[11,14,16,17] representing more conventional polymer architectures. Those structures have a point of commonality in that their low-**Q** gradient is about -2. The Beaucage form factor has been designed to describe arbitrary mass fractals including polymers. In the low-**Q** range this approach yields a fractal aggregate of dimension $P \cong 3$ and signals the presence of a very dense 3-dimensional system, e.g., a branched polymer "bottle brush". Examples of possible structures[39] are given in Figure 9. A potential mechanism of branching for the "living" polymers supramolecular structure could come about if

lithium increases its coordination number. Similar values of P have been found for aerogels, foams, or aggregating silica particles.[20,40] The values of P and R_g (ca. 10^3 Å) are independent of polymer concentration. This may be seen particularly well in Figure 10, where the residual low-**Q** scattering after the subtraction of the corresponding form factors for the dimer tetramer mixtures are shown for all concentrations. The aggregation behavior reported in this work has precedence in the self-assembling characteristics of benzyllithium in the solid state[41,42] where the head groups form stacked arrays.

Conclusions

SANS data from living polymers with styryllithium head groups display structures over a wide **Q** range ($10^{-3} \leq \mathbf{Q} \leq 10^{-1}$ Å^{-1}), indicating the presence of different length scales that signify the structures obtained from polymer aggregation. In the mid-**Q** range ($\mathbf{Q} \geq 0.2$ Å^{-1}) the concentration dependent data could be quantitatively analyzed in the form of a mixture of dimers and tetramers. The relative volume fraction of the tetramers, being the only adjustable parameter, increases with decreasing monomer volume fraction. Aside from these low functionality aggregates, large scale structures are present with sizes above 1000 Å. Their scattering behavior can be described by a form factor for mass fractals recently proposed by Beaucage. The measured fractal dimension of $P \cong 3$ indicates dense aggregated objects like branched "bottle brushes". It could be estimated from the absolute intensities that only a minute fraction of the monomers present participates in the large scale aggregates ($\sim 10^{-4}$). The observed structural variety of the living poly(styryllithium) solution entities shows that the morphology of these living polymer systems is more complex than that promoted by the entrenched textbook[4] mechanism of anionic polymerization in a hydrocarbon milieu.

References and Notes

(1) Fetters, L. J.; Balsara, N. P.; Huang, J. S.; Jeon, H.; Almdal, K.; Lin, M. Y. *Macromolecules* **1995**, *28*, 4996.
(2) Worsfold, D. J.; Bywater, S. *Can. J. Chem.* **1960**, *38*, 1981.
(3) van Beylen, M.; Bywater, S.; Smets, G.; Szwarc, M.; Worsfold, D. J. *Adv. Polym. Sci.* **1988**, *86*, 87.
(4) Szwarc, M. *Ionic Polymerization Fundamentals*; Hanser/Gardner Publishers: Cincinnati, OH, 1996.
(5) Morton, M.; Fetters, L. J. *Rubber Chem. Technol.* **1975**, *48*, 359.
(6) Gilman, H.; Cartledge, F. J. *Organomet. Chem.* **1964**, *2*, 447.
(7) Bach, R. O.; Kamienski, C. W.; Ellested, R. B. *Encycl. Chem. Technol.* **1967**, *12*, 529.
(8) Kirste, R.; Kruse, W. A.; Schelten, J. *Makromol. Chem.* **1972**, *162*, 299.
(9) Fetters, L. J.; Hadjichristidis, N.; Lindner, J. S.; Mays, J. W. *J. Phys. Chem. Ref. Data* **1994**, *23*, 619.
(10) J. S. Higgins; H. C. Benoit *Polymers and Neutron Scattering*; Clarendon Press, Oxford, U.K., 1994.
(11) Debye, P. J. *Phys. Colloid Chem.* **1947**, *51*, 18.
(12) Benoît, H. *J. Polym. Sci.* **1953**, *11*, 507.
(13) Dozier, W. D.; Huang, J. S.; Fetters, L. J. *Macromolecules* **1991**, *24*, 2810.
(14) Cassasa, E.; Berry, G. *J. Polym. Sci., Polym. Phys. Ed.* **1966**, *4*, 881.
(15) Weiss, E. *Angew. Chem., Int. Ed. Engl.* **1993**, *32*, 1501. See also: Lambert, C.; Schleyer, P. v. R. *Angew. Chem., Int. Ed. Engl.* **1994**, *33*, 1129.
(16) Egelhaaf, S. U.; Schurtenberger, P. *J. Phys. Chem.* **1994**, *98*, 8560.
(17) Brulet, A.; Boué, F.; Cotton, J. P. *J. Phys. II Fr.* **1996**, *6*, 885.
(18) Beaucage, G.; Schaefer, D. *J. Non-Cryst. Solids* **1994**, *172*−*174*, 797.
(19) Beaucage, G. *J. Appl. Crystallogr.* **1995**, *28*, 717.
(20) Beaucage, G. *J. Appl. Crystallogr.* **1996**, *29*, 134.
(21) de Gennes, P. G. *Scaling Concepts in Polymer Physics*; Cornell University Press: Ithaca, NY, 1979.
(22) Huber, K.; Buntle, S.; Lutz, P.; Burchard, W. *Macromolecules* **1985**, *18*, 1461.
(23) Grest, G.; Fetters, L. J.; Huang, J. S.; Richter, D. *Adv. Chem. Phys.* **1996**, *94*, 67.
(24) *Developments in Ionic Polymers*; Wilson, A. D., Prosser, H. J., Eds.; Applied Science: London, 1983; Vol. 1.
(25) *Structure and Dynamics of Strongly Interacting Colloids and Supramolecular Aggregates in Solution*; Chen, S.-H., Huang, J. S., Tartaglia, P., Eds.; Series C: Mathematical and Physical Sciences; Kluwar Academic Publishers: Dordrecht, The Netherlands, 1992; Vol. 369, p 26.
(26) Halperin, A.; Tirrell, M.; Lodge, T. E. *Adv. Polym. Sci.* **1992**, *100*, 31.
(27) Hommes, N. J. R.; Buhl, M.; Schleyer, P. v. R. *J. Organomet. Chem.* **1991**, *409*, 307.
(28) Sapse, A.-M.; Jain, D. C.; Raghavachari, K. In *Lithium Chemistry: A Theoretical and Experimental Overview*, Sapse, A.-M., Schleyer, P. v. R., Eds.; John Wiley and Sons: New York, 1995; p 45. Sapse et al. concluded (for hydrocarbon milieu) that "it is doubtful that the monomeric species can exist except under very unusual circumstances". A similar conclusion was reached by Brown in 1966: Brown, T. L. *J. Organomet. Chem.* **1966**, *5*, 191.
(29) Stellbrink, J.; Willner, L.; Richter, D.; Fetters, L. J.; Huang, J. S. To be submitted.
(30) Worsfold, D. J.; Bywater, S. *Macromolecules* **1972**, *5*, 393. This reference reported an association state of 2 ± 0.1 (based upon five different molecular weights) for the styryllithium head groups in cyclohexane; a value in apparent pleasing confluence with that dictated by mechanistic beliefs. As mentioned, the color of active head group solutions prohibits the attainment of quantitative molecular weights. Additional dual difficulties are the scattering contributions from the variable populations of dimers and tetramers along with the alterations in the concentration and size of the large scale aggregates. Representative scattering data from the styryllithium solutions were not presented.
(31) Johnson, A. F.; Worsfold, D. J. *Makromol. Chem.* **1965**, *85*, 273. It is asserted in ref 4, p 35, that "the (styryllithium) absorption is weak in aliphatic solvents and $\lambda_{max} > 400$ nm". In reality, λ_{max} varies (depending upon the identity of the solvent and counterion) from 328 to 345 nm. See Table 5 (p 89) of: Szwarc, M. *Adv. Polym. Sci.* **1983**, *49*, 1. The 328 nm wavelength was used by the authors of ref 30 "to monitor the polystyryllithium concentration".
(32) Willner, L.; Jucknischke, O.; Richter, D.; Farago, B.; Fetters, L. J.; Huang, J. S. *Europhys. Lett.* **1992**, *19*, 297.
(33) Richter, D.; Jucknischke, O.; Willner, L.; Fetters, L. J.; Lin, M.; Huang, J. S.; Roovers, J.; Toporowski, P. M.; Zhou, L. L. *J. Phys. IV, Colloq. C8, Suppl. J. Phys.* **1993**, *3*, 3.
(34) Willner, L.; Jucknischke, O.; Richter, D.; Roovers, J.; Zhou, L. L.; Toporowski, P. M.; Fetters, L. J.; Huang, J. S.; Lin, M.; Hadjichristidis, N. *Macromolecules* **1994**, *27*, 3821.
(35) Fetters, L. J.; Huang, J. S.; Young, R. N. *J. Polym. Sci., Polym. Chem. Ed.* **1996**, *34*, 1517.
(36) Fetters, L. J.; Huang, J. S.; Stellbrink, J.; Willner, L.; Richter, D. *Macromol. Chem., Symp.* **1997**, *121*, 1.
(37) Daoud, M.; Stanley, H. E.; Stauffer, D. In *Physical Properties of Polymers Handbook*; Mark, J., Ed.; AIP Press: Woodbury, NY, 1996; p 71.
(38) Adam, M.; Lairez, D. *Fractals* **1993**, *1*, 149.
(39) The Eden, Vold, and Witten-Sander fractal structures were reproduced from Figure 2 of: Schaefer, D. W. *Science* **1989**, *243*, 1023. See also: Schaefer, D. W. *Mater. Res. Soc. MRS Bull.* **1988**, *XIII*, 22.
(40) Keefer, K. D.; Schaefer, D. W. *Phys. Rev. Lett.* **1986**, *56*, 2376.
(41) Pattermann, S. P.; Karle, I. D.; Stucky, G. D. *J. Am. Chem. Soc.* **1970**, *92*, 1150.
(42) Beno, M. A.; Hope, H.; Olmstedt, M. M.; Power, P. P. *Organometallics* **1985**, *4*, 117.

MA971890E